# Smoothed Particle Galerkin Method with a Momentum-Consistent Smoothing Algorithm for Coupled Thermal-Structural Analysis

X. Pan[1*], C.T. Wu[1], W. Hu[1], Y.C. Wu[1]
*1Livermore Software Technology Corporation*
*7374 Las Positas Road, Livermore, CA 94550, USA*

## Abstract

*This paper introduces a momentum-consistent smoothing algorithm to Smoothed Particle Galerkin (SPG) method [1] in LS-DYNA for the coupled thermal-structural analysis. In contrast to the kernel approximation in conventional Lagrangian particle methods, the system of equations of the present method is discretized and approximated following that in the SPG method. The momentum-consistently smoothing algorithm provides the desired stability and accuracy in the thermal structural coupling applications. Furthermore, the algorithm is coupled with FEM with sharing nodes to increase the computational efficiency. Two benchmarks including heat flux and thermal expansion are studied to demonstrate the accuracy of the present method. In addition, the frictional drilling test is simulated to demonstrate the effectiveness of the proposed method in the coupled thermal-structural analysis involving material failure.*

*Keywords: particle, Galerkin, nodal integration, frictional drilling, moment consistent*

## Introduction

In the past two decades, particles methods have drawn a lot of attention in the solid and structural analysis, because they offer many numerical advantages over conventional numerical methods such as the finite element method (FEM). Although the Lagrangian FEM has been widely used in the solid and structural analysis since early 1940s, it suffers from the issues of convergence and element distortion in the simulation of large deformation and material failure problems. In 1998 Monaghan [2] introduced a particle method—Smoothed Particle Hydrodynamics (SPH), which was originally developed for the large deformation analysis of astrophysical problems. Since the SPH functions are evaluated only at the particles, it is unnecessary to use any meshes and thus overcoming the drawbacks of the finite element method in large deformation applications. Nevertheless, it is well-known that SPH suffers from several numerical instabilities such as approximation inconsistency, tension instability, spurious low-energy modes and the inability in the material failure analysis when it is applied to solid and structural analysis.

Different versions of particle methods have been developed to resolve the SPH instabilities in solid and structural analysis. Nevertheless, most particle methods are based on the nodal integration scheme and still suffer from the spurious zero modes and the tensile instability problems. Chen et al. proposed a Stabilized Conforming Nodal Integration (SCNI) method [3], in which a strain smoothing scheme was introduced as a stabilization process to improve the spurious low-energy modes. Wu et al. [1,4-6] derived a new formulation based on a smoothed displacement field within the meshfree Galerkin variational framework and was called the Smoothed Particle Galerkin (SPG) method [7-10]. The SPG discretized system of equations is integrated at the nodes and effectively bypass most numerical instabilities in conventional particle methods for solid and structural analysis. The SPG method been successfully applied to the simulation of ductile and semi-brittle material failure problems in manufacturing and high velocity impact applications [7-10].

In this paper, we proposed a new smoothing algorithm for the SPG method in coupled thermal-structural analyses. In essence, a second-order accurate momentum-consistent algorithm is developed for SPG method to provide the desired stability and accuracy in the thermal-structural coupling applications. The detailed formulation for the new smoothing algorithm will not be emphasized here and can be referred to [11].

## LS-DYNA Keyword of the SPG with Momentum Consistently Smoothing Algorithm

Smoothed Particle Galerkin method with the Momentum-Consistent Smoothing algorithm has been implemented for 3D solid element formulation 47 in the keyword *SECTION_SOLID_SPG for the explicit dynamics analysis. Since the SPG nodes are automatically generated from the nodes of the users' FEM input (4/6/8-noded solid element), only a change in the FEM section keyword is needed. The input deck format of *SECTION_SOLID_SPG for card 2 and card 3 is described as follows:

| Card 2 | **DX** | **DY** | **DZ** | ISPLINE | **KERNEL** | LSCALE | SMSTE | SUKTIME |
|---|---|---|---|---|---|---|---|---|
| Default | 1.5 | 1.5 | 1.5 | 0 | 0 | 0 | 15 | 0 |
| Card 3 | IDAM | SF | STRETCH | **ITB** | | | | |
| Default | 0 | 0 | 1.2 | 1 | | | | |

DX,DY,DZ — Normalized dilation parameters of the kernel function in X, Y and Z directions, the recommend range in SPG is 1.4~1.8

KERNEL — Kernel type. KERNEL=0 updated Lagrangian(UL) kernel, KERNEL=1 Eulerian (E) kernel, and KERNEL=2 pseudo-Lagrangian (PL) kernel.

ITB — Stabilization parameter**, ITB=3** for Momentum Consistently Smoothed Particle Galerkin method.

## LS-DYNA Keyword of the Explicit Thermal Structural Analysis

The parameters for the explicit thermal analysis is in the keyword *CONTROL_THERMAL_TIMESTEP. The following is a snapshot of *CONTROL_THERMAL_TIMESTEP card 1

| Card 1 | TS | **TIP** | **ITS** | TMIN | TMAX | DTEMP | TSCP | LCTS |
|---|---|---|---|---|---|---|---|---|
| | 0 | 0.0 | 1.0e-4 | 0 | 0 | 0 | 0 | 0 |

TIP — **0.0** is used for explicit analysis

ITS — Time step for the explicit thermal analysis, it should be larger than the mechanical time step, and usually taken as 10 times of the mechanical time step.

## Numerical Examples

**Heat Flux**

This example is analyzed to verify the accuracy of our algorithm in the application of heat transfer. A metal block with a length of 0.25, width and height of 0.03 is used for the simulation. The heat flux boundary is applied on the right surface of the block, and the heat flux is set as -1.0E5. The dimensionless unit is employed in the study.

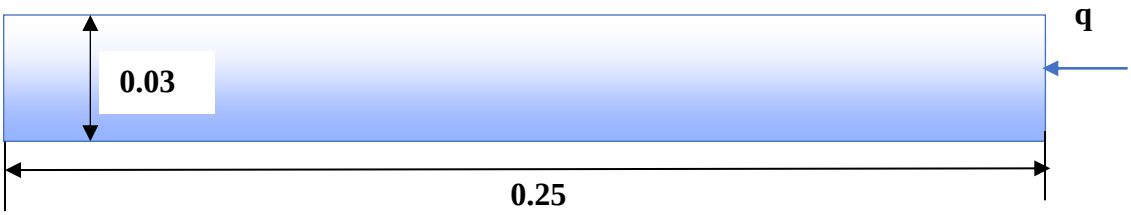


**Figure 1**: Geometry for the simulation

The material law of Johnson Cook model and Gruneisen equation of state is used in the simulation. The corresponding input for LS-DYNA is as following:

```
*MAT_JOHNSON_COOK_TITLE
6061-T6, kg, m, s, Pa, N
$#     mid        ro         g         e        pr       dtf        vp    rateop
      2701 2.700E+11 26.923E+9 7.000E+10  0.300000     0.000     0.000     0.000
$#       a         b         n         c         m        tm        tr      epso
  324.1E+6  113.8E+6      0.42     0.002      1.34     925.0     293.0       1.0
$#      cp        pc     spall        it        d1        d2        d3        d4
    1256.0   -1.0E20       2.0       0.0      0.00      0.00      0.00       0.0
$#      d5      c2/p      erod     efmin
$      1.6       0.0         1     0.001
       0.0       0.0         1     0.001
*EOS_GRUNEISEN_TITLE
eos1, m/s
$#   eosid         c        s1        s2        s3     gamao         a        e0
      2701 4.648E-01       1.4       0.0       0.0      1.97       0.0       0.0
```

Three models are used for the simulation, a), the both left and right half parts of the block are modeled with SPG, and it is called SPG-SPG model. b), the both parts are modeled with FEM, it is called FEM-FEM model and used as reference. c), the left part is modeled with FEM, while the right is modeled with SPG, it is called FEM-SPG model. The different parts share the same nodes at the interface. The detailed models are shown in Figure 2.

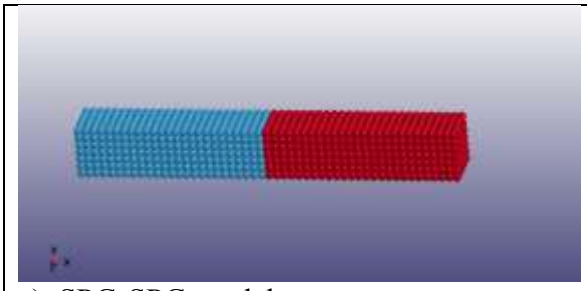

a), SPG-SPG model

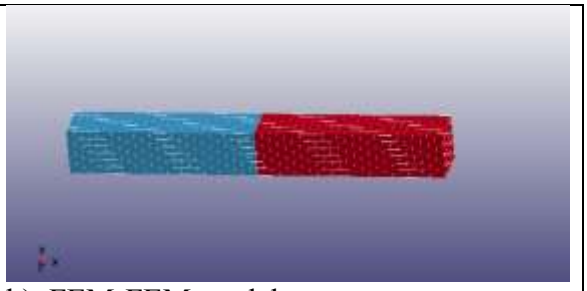

b), FEM-FEM model

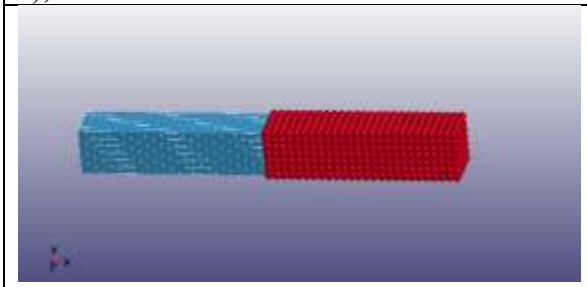

c), FEM-SPG model

**Figure 2**: Three models used for the simulation

Figure 3 shows the temperature contours at time t=300. There are only little differences of the maximum and minimum temperatures among the three models, and the temperature transitions are also very smooth near the interfaces in SPG-SPG model and FEM-SPG model, just as that in FEM-FEM model.

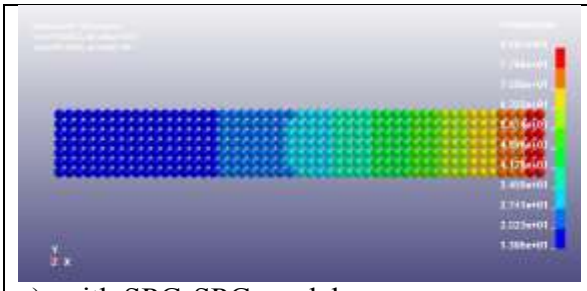

a), with SPG-SPG model

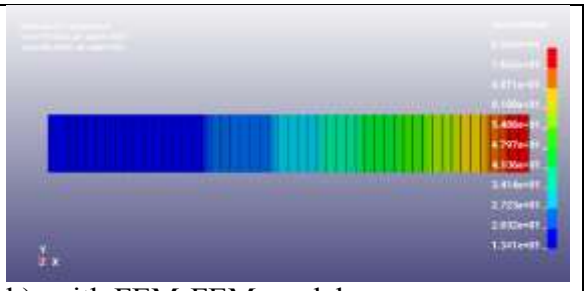

b), with FEM-FEM model

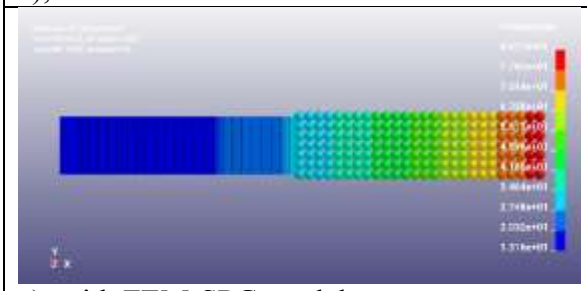

c), with FEM-SPG model

**Figure 3**: Temperature contours at t=300 with different models

To compare the results quantitively, the temperature histories at three positions are measured: Position 1 locates at the ¼ length to the right surface, Position 2 locates at the ½ length to the right surface, and Position 3 locates ¼ length to the left surface. Figure 4 shows the curves of the temperature-time histories at the three positions with 3 models, and they agree very well.

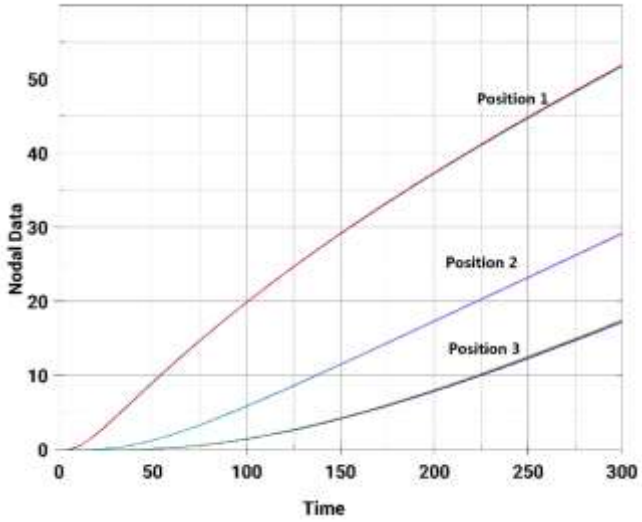


**Figure 4**: Temperature-time histories at three positions.

**Thermal Expansion**

The heat transfer and thermal expansion simulation is conducted in this example. The metal block has a size of

$0.09 \times 0.03 \times 0.01$. The temperature boundary condition is applied on the lower surface of the block is applied, and the corresponding temperature time history curve is shown in Figure 5.

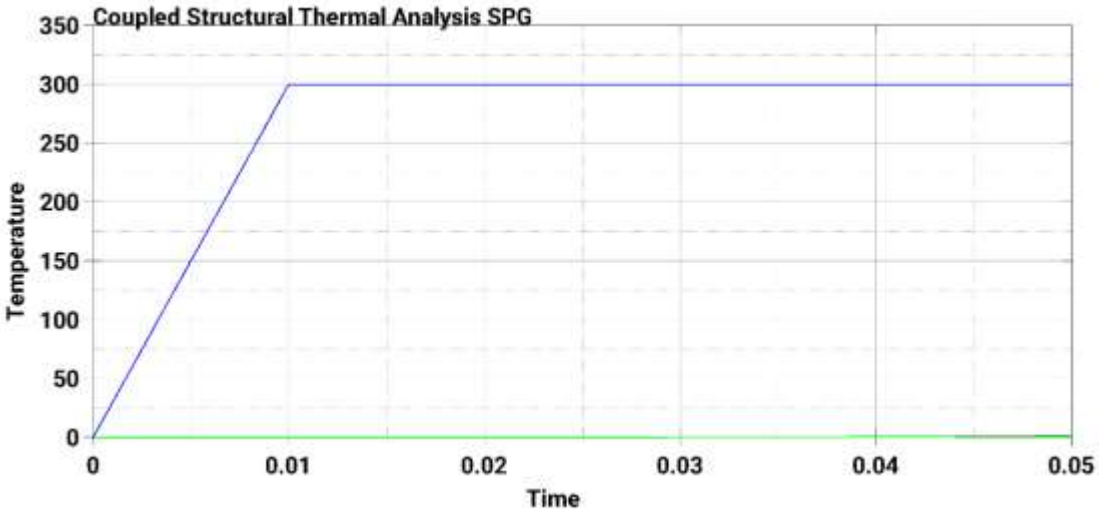


**Figure 5**: The applied temperature value at the block bottom

The Johnson Cook model and Gruneisen equation of state is used as for the simulation, the corresponding input for Ls Dyna is as following:

```
*MAT_JOHNSON_COOK_TITLE
6061-T6, kg, m, s, Pa, N
$#     mid        ro         g          e        pr       dtf        vp    rateop
       6061 2.7000E+5 26.923E+9 7.000E+10  0.300000     0.000     0.000     0.000
$#       a          b         n          c         m        tm        tr      epso
 3.241E+08  1.138E+80.41999999     0.002      1.34     925.0     293.0       1.0
$#      cp         pc     spall         it        d1        d2        d3        d4
$    1256.0-1.0000E20       2.0        0.0     -0.77      1.45     -0.47       0.0
     1256.0-1.0000E20       2.0        0.0      0.00      0.00      0.00       0.0
$#      d5       c2/p      erod     efmin
$      1.6        0.0         1     0.001
       0.0        0.0         1     0.001
*EOS_GRUNEISEN_TITLE
eos1, m/s
$#   eosid          c         s1         s2         s3     gamao          a         e0
       6061 464.81001        1.4        0.0        0.0      1.97        0.0        0.0
$ c: bulk sound speed, defined as: sqrt(K/rho)
$    K: bulk modulus, rho: density
$#       v0
       1.0
```

Three models are used for the simulation: a), both the lower and upper parts are modeled with SPG, it is called SPG-SPG model. b), both parts are modeled with FEM, and it is called FEM-FEM model. c), the lower part is modeled with FEM, while the upper part is modeled with SPG, and it is called FEM-SPG model. Different parts share the same nodes at the interface. The detailed modeling is shown in Figure 6.

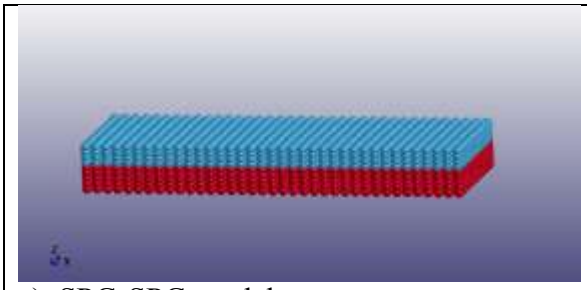

a), SPG-SPG model

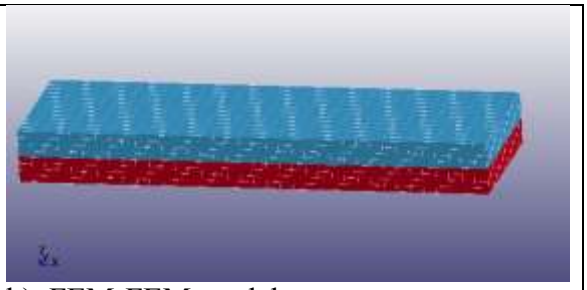

b), FEM-FEM model

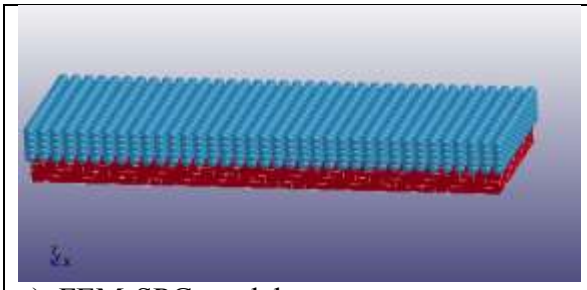

c), FEM-SPG model

**Figure 6**: Three models for the simulation

The temperature contours with the three models at time t=0.05 are plotted in Figure 7, and they look very similar. The temperature history is measured at two positions: Position 1 locates at the ¼ height to the top of the block, and Position 2 locates at the ½ height to the top of the block. Figure 8 shows the temperature histories with different models, and they agree well. The difference is larger than that in the heat flux example, because much less nodes in the z direction are used for the simulation.

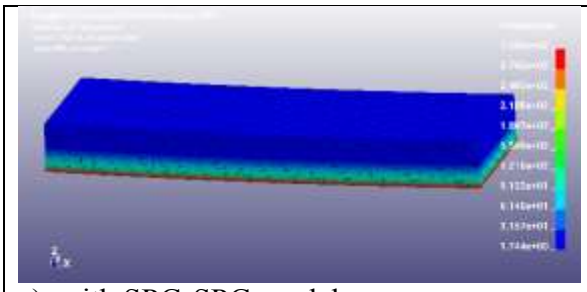

a), with SPG-SPG model

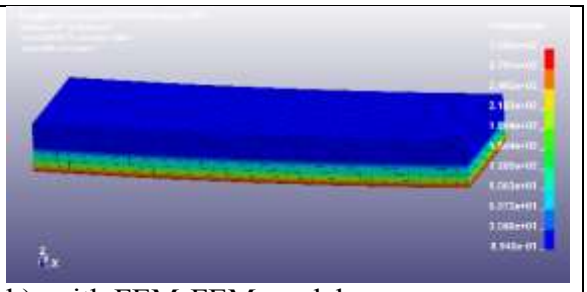

b), with FEM-FEM model

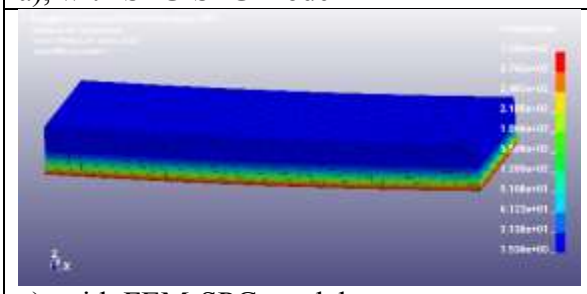

c), with FEM-SPG model

**Figure 7**: The temperature contours at time t=0.05

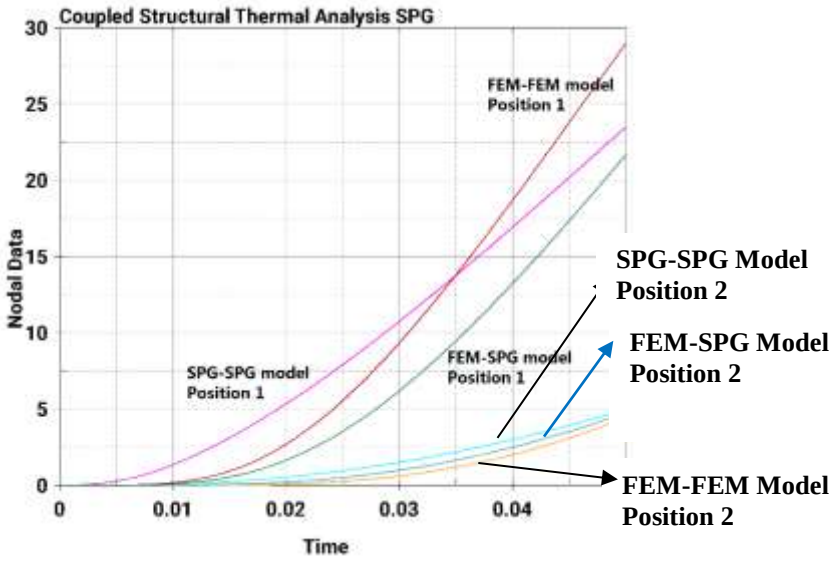


**Figure 8**: Temperature history measured at position 1 and position 2

The block is deformed due to the temperature gradient, and the corresponding z displacement contours are plotted in Figure 9. The results from SPG-SPG and FEM-SPG are comparable to that from FEM-FEM. No rigid motion and spurious zero-energy mode are observed in our simulation.

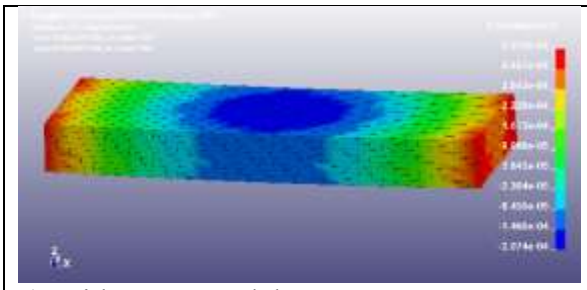

a), with -SPG model

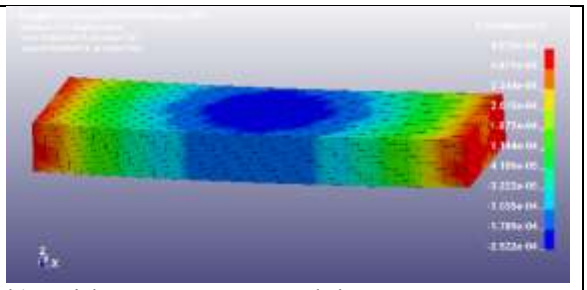

b), with FEM-FEM model

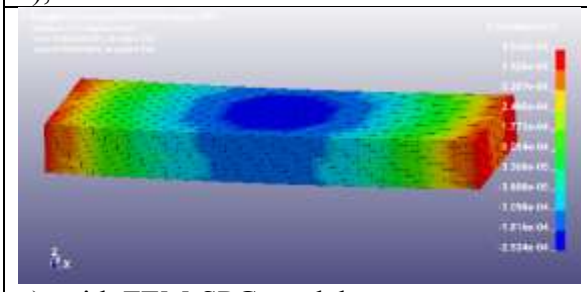

c), with FEM-SPG model

**Figure 9**: Z displacement contours with different models.

**Frictional Drilling**

Non-traditional drilling and thread tapping processes such as frictional drilling has become more and more popular in the automotive industry, furniture manufacturing and other applications. This is because the traditional drilling applicability is very complicated and difficult due to insufficient thickness of a workpiece. The frictional drilling is a new process usually carried out using a special tungsten tool. Under the frictional contact between the tungsten tool and the workpiece, the workpiece metal becomes soften due to the significant increased temperature in the drilling zone. Subsequently, the tool can easily penetrate through the workpiece and produce the desired bushing for the following screwing process. Up to now, the majority of the studies on the frictional drilling is focused on the experiments [12-14] because of the numerous challenges for this kind of simulation. The major numerical challenge is subjected to the large material deformation and damage occurring during the drilling process. The numerical simulation is very difficult to be conducted using the existing numerical approaches. There are some studies [14,15] using the finite element method where the element erosion technique has to be used because the finite elements are distorted severely with the material deformation. The element erosion technique in FEM leads to the mass conservation problems and therefore the desired bushing formation phenomena cannot be accurately simulated. The formation of the bushing shape is one of the key features of the frictional drilling process that has to be produced in the numerical simulation.

In this paper, the SPG with Momentum-Consistent Smoothing algorithm is used for the simulation. The dimension of the tool, simulated mesh and boundary condition is shown in Figure 10 and 11. The workpiece (AISI 304 Steel) was created as a disk of 18mm diameter and 1.5mm thickness. The center part of 6.4mm diameter of the disk is modeled with SPG, while the rest part is modeled with FEM. The mechanical mass of the workpiece is scaled with 40,000 to obtain a larger integration time step in the explicit dynamic analysis.

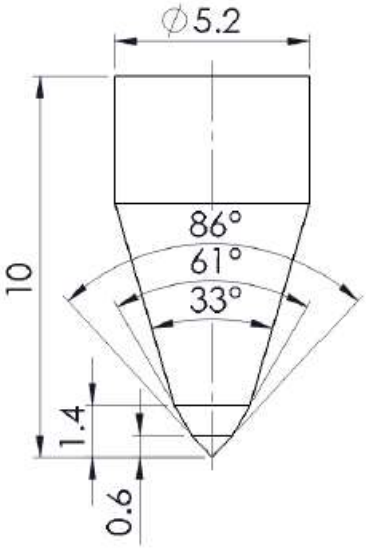


**Figure 10**: The dimension of the tool.

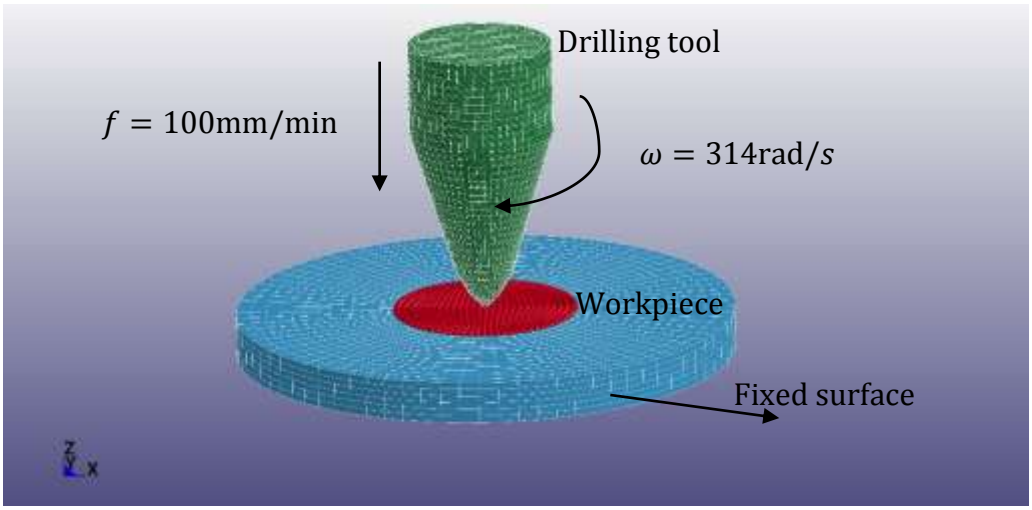


**Figure 11**: The simulated mesh and boundary condition.

Material properties and Johnson-Cook parameters are used for the simulation, the parameters are referred to [14] and listed in Table 1.

| Parameter | Units | Value |
|---|---|---|
| Young Modulus | MPa | 193.0 |
| Poisson ratio | | 0.3 |
| Mechanical density | $N/m^3$ | 3.2E08 |
| Thermal density | $N/m^3$ | 8.0E03 |
| Melting temperature | K | 1673 |
| Room temperature | K | 316 |
| Specific heat capacity | J/(kgK) | 500 |
| Heat transfer coefficient | W/(mK) | 162 |
| Thermal expansion | $10^{-6}K^{-1}$ | 18.4 |
| Initial yield strength A | MPa | 280 |
| Hardening modulus B | MPa | 802.5 |
| Strain hardening exponent n | | 0.622 |

| | | |
|---|---|---|
| Thermal softening exponent m | | 1.0 |
| Strain rate constant C | | 0.0799 |
| Reference strain rate | 1/s | 1.0 |

Table 1: AISI 304 steel properties and Johnson-Cook parameters

Figure 12 and 13 show the equivalent plastic strains at different tool traveling distances. The temperature contours at different travel distances are shown in Figure 14. Our simulation exhibits at least the following merits:

1. No element erosion is used, and the mass of system is conservative. As a result, the bushing can be obviously produced in the simulation as observed in the experiment.
2. The spurious low energy mode is well controlled.
3. Both strain and temperature fields are very smooth, even at the very large deformation zone.
4. The transition of the strain and temperature fields near the FEM-SPG interface is very smooth.

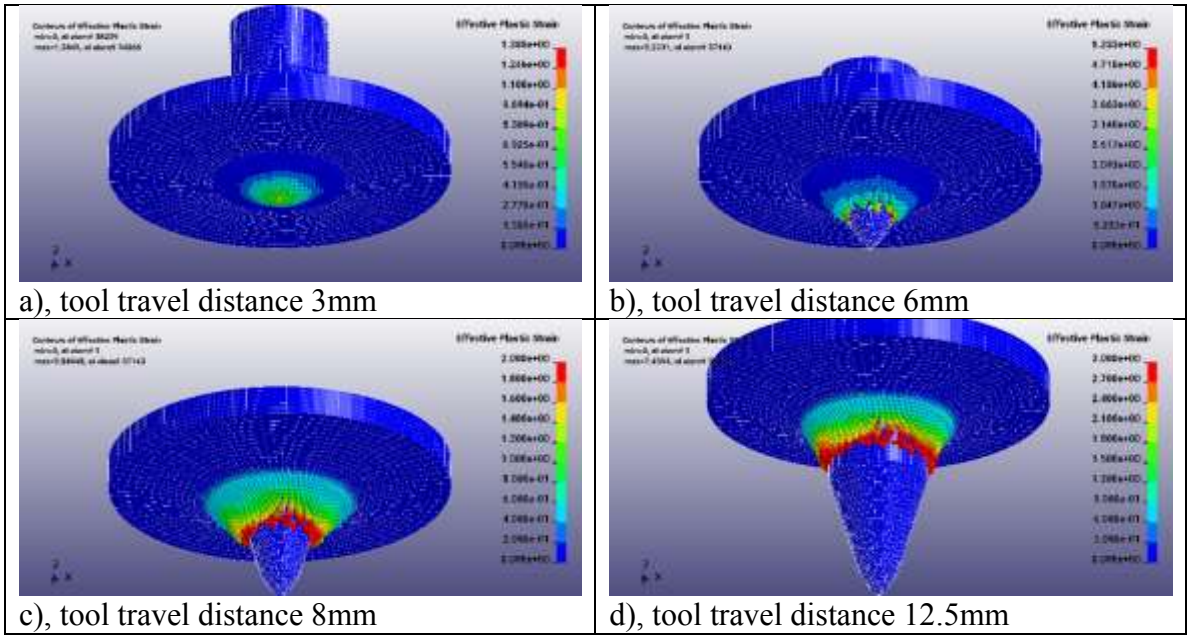

a), tool travel distance 3mm

b), tool travel distance 6mm

c), tool travel distance 8mm

d), tool travel distance 12.5mm

**Figure 12**: Equivalent plastic strain in the workpiece at different tool travel distances, global view.

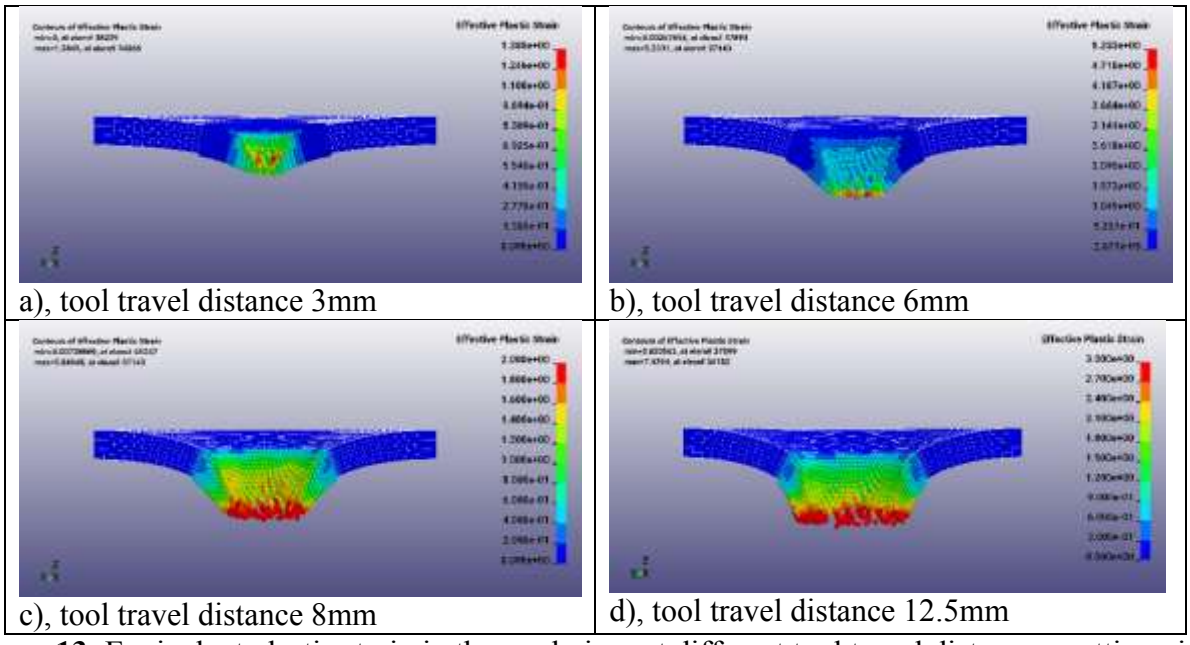

a), tool travel distance 3mm

b), tool travel distance 6mm

c), tool travel distance 8mm

d), tool travel distance 12.5mm

**Figure 13**: Equivalent plastic strain in the workpiece at different tool travel distances, cutting view.

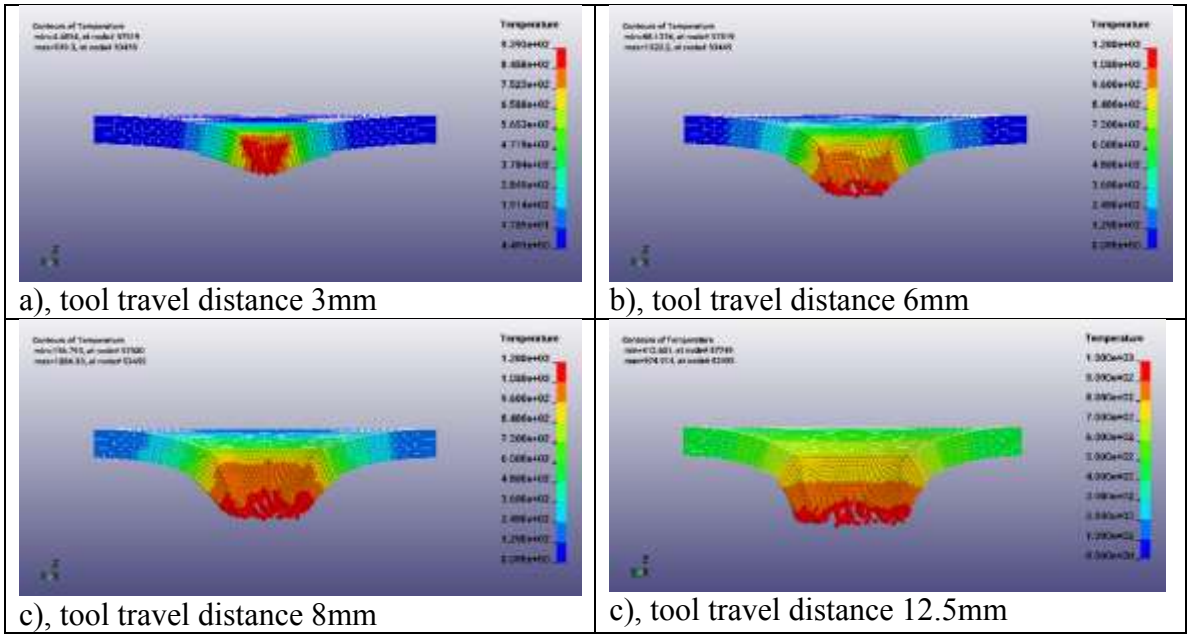

a), tool travel distance 3mm

b), tool travel distance 6mm

c), tool travel distance 8mm

c), tool travel distance 12.5mm

**Figure 14**: Workpiece temperature plots at different tool travel distances.

## Conclusion

A momentum-consistent smoothing algorithm was developed for the Smoothed Particle Galerkin (SPG) method. The new algorithm provides the desired stability and accuracy in the thermal-structural coupling applications. Furthermore, the algorithm is coupled with FEM with sharing nodes to increase the computational efficiency. Our benchmark tests verified the accuracy of the present method in the thermal-structural analysis. It is worthwhile to note that the SPG method has demonstrated it attractive capability in the frictional drilling simulation. The further investigation of the new method in other industrial applications will be reported in the near future.

## References


[1] C.T. Wu, M. Koishi, W. Hu, A displacement smoothing induced strain gradient stabilization for the meshfree Galerkin nodal integration method, Computational Mechanics, 56 (2015):19-37.

[2] J.J. Monaghan, An introduction to SPH, Computational Physics Communication, 48(1988):89-96

[3] J.S. Chen, C.T. Wu, S. Yoon, Y. You, A stabilized conforming nodal integration for Galerkin meshfree methods, International Journal of Numerical Methods in Engineering, 85(2001) 435-466.

[4] C.T. Wu, Y.C. Wu, M. Koishi, A strain-morphed nonlocal meshfree method for the regularized particle simulation of elastic-damage induced strain localization problems, Computational Mechanics, 56(2015) :1039-1054

[5] C.T. Wu, N. Ma, K. Takada, H. Okada, A meshfree continuous-discontinuous approach for the ductile fracture modeling in explicit dynamics analysis, Computational Mechanics, 58(2016):391-409.

[6] Y.C. Wu, D.D. Wang, C.T. Wu, H.J. Zhang, A direct displacement smoothing meshfree particle formulation for impact failure modeling, International Journal of Impact Engineering. 87 (2017):169-185.

[7] C. T. Wu, T.Q. Bui, Y. Wu, T.L. Luo, M. Wang, C.C. Liao, P.Y. Chen, Y.S. Lai. Numerical and experimental validation of a particle Galerkin method for metal grinding simulation, Computational Mechanics. https://doi.org/10.1007/s00466-017-1456-6, 2017, accepted for publication.

[8] C. T. Wu, Y. Wu, J.E. Crawford, J.M. Magallanes. Three-dimensional concrete impact and penetration simulations using the smoothed particle Galerkin method, International Journal of Impact Engineering 106 (2017): 1-17.

[9] Y. Wu, C. T. Wu Simulation of impact penetration and perforation of metal targets using the smoothed particle Galerkin method, Journal of Engineering Mechanics 2017, accepted for publication.

[10] X. F. Pan, C. T. Wu, W. Hu, Y. C. Wu, A Smoothed Particle Galerkin Method with a Momentum Consistent Algorithm for Thermal Structural Analysis. To be submitted to Internal Journal for Numerical Methods in Engineering.

[11] H.M. Chow, S.M, Lee, L.D. Yang, Machining characteristic study of friction drilling on AISI 304 stainless steel, Journal of Materials Processing Technology, 207(2018):180-186

[12] S.M. Lee, H.M. Chow, F.Y Huang, B.H. Yan, Friction drilling of austenitic stainless steel by uncoated and PVD AlCrN- and TiAlN-coated tungsten carbide tools. International Journal of Machine Tools and Manufacture 49(2009):81-88
[13] P. Krasauskas, S. Kilikevicius, R. Cesnavicius, D. Pacenga, Experimental analysis and numerical simulation of the strainless AISI 304 steel friction drilling process, Mechanika, 20(2014):590-595
[14] Thermo-Mechanical Finite Element Modeling of the Friction Drilling Process, S.F. Miller, A.J. Shih, Journal of Manufacturing Science and Engineering, 129(2007):531-538